JMEPEG (2018) 27:2960–2966
https://doi.org/10.1007/s11665-018-3397-4

1059-9495/$19.00

Effect of Sintering Temperature on Density and Mechanical Properties of Solid-State Sintered Silicon Carbide Ceramics and Evaluation of Failure Origin

Dulal Chandra Jana, Prasenjit Barick, and Bhaskar Prasad Saha

(Submitted May 5, 2017; in revised form March 23, 2018; published online May 15, 2018)

Densified silicon carbide (SiC) is prepared through dry pressing of SiC powder followed by pressureless sintering in the presence of boron carbide and carbon as the additives. Sintering of SiC parts shows the increase in density with the increase in temperature (1950-2180 °C) by resulting in higher than 98% relative density (RD) at 2150 °C and above for 1 h. Sintered specimens are evaluated concerning the phase, microstructure and mechanical properties including hardness and flexural strength. The machined surface of SiC parts with about 98% RD is studied for the origin of failure. The estimated size of critical flaws (32-110 µm) based on flexural strength and fracture toughness indicates that machining defects are one of the primary reasons for failure in SiC ceramics. The order of magnitude of defects on machined surfaces of sintered SiC by SEM studies is found to be comparable with the estimated size of critical flaws. The failure behavior of SiC is discussed with the help of Weibull statistics with respect to the variation of four-point flexural strength.

Keywords fracture toughness, mechanical properties, silicon carbide (SiC), Weibull statistics and surface cracks

1. Introduction

Silicon carbide is a non-oxide ceramic material with superior mechanical properties such as high strength, moderate fracture toughness, high wear resistance and capability of retaining strength at high temperature, in combination with the excellent thermal properties and very high chemical inertness (Ref 1). Therefore, it has been considered as high-temperature structural ceramics for several applications including gas turbines, industrial heat exchangers, diesel engines, mechanical seals, abrasives and many other devices (Ref 1-5). The development of advanced ceramics based on SiC is also technologically important in a wide range of applications such as structural material in telescopes for space exploration, synchrotron optical elements, biomaterials, high-temperature semiconductors, etc.

Densification of SiC powder compacts can be achieved by the use of Y_2O_3/Al_2O_3 additives (Ref 4, 6). These additives become liquid phase at high temperature and assist in the densification to near theoretical density through particles rearrangement and solution re-precipitation mechanisms. However, the presence of high-temperature liquid phase has a deleterious effect on high-temperature strength and creep resistance of SiC (Ref 7). High-density SiC parts can also be made through a reaction bonding process (Ref 8, 9) in which densification is achieved through the formation of Si_3N_4 or SiC by the reaction between molten silicon and N_2 (in reaction atmosphere) or C (in the green preform), respectively. SiC parts made through the reaction bonding process also suffer from deleterious effect at high temperature as the application temperature approaches the melting point of silicon. In addition to that, SiC parts made by the reaction bonding process exhibit inhomogeneously distributed free silicon, which lowers the strength and other properties (Ref 9). Prochazka (Ref 10) of General Electric, in 1975, discovered the solid-state sintering of SiC and demonstrated the sintering of SiC in the absence of a substantial amount of liquid phase using B and C as the additives. Solid-state sintered SiC (S-SiC) ceramics offer advantages in terms of their superior strength at ambient as well as elevated temperature compared to the liquid-phase sintered and reaction bonded silicon carbide.

The flow sheet diagram for processing of S-SiC ceramics by powder metallurgy technique is shown Fig. 1. The process involves shaping of green bodies by dry pressing SiC powder premixed with binder/additives followed by low temperature (~ 500 °C) heat treatment for the removal of organic volatiles and the increase in green strength for handling and machining purposes. Subsequently, SiC parts are sintered at high temperature and machined to final shape and required dimensions. The primary limitation of S-SiC for structural applications is the variability of strength due to the existence of flaw size distribution. The origin of defects could be for several reasons: surface cracks that can arise from machining operations or even by handling, and internal defects including pores, weak interfaces, inclusions, etc. There are many studies on the mechanical properties of SiC ceramics but only a few of them correlate their mechanical properties with the strength reliability and failure origin. Mechanical properties of liquid-phase sintered and siliconized SiC at ambient as well as elevated temperature are reported in the literature (Ref 6, 11-13). Also, the mechanical properties improvements in liquid-phase sintered SiC ceramics through the control of microstructure are reported elsewhere (Ref 7, 14, 15).

Dulal Chandra Jana, Prasenjit Barick, and **Bhaskar Prasad Saha**, Centre for Non-Oxide Ceramics, International Advanced Research Centre for Powder Metallurgy & New Materials (ARCI), RCI Road, Balapur PO, Hyderabad 500005, India. Contact e-mail: janad@arci.res.in.

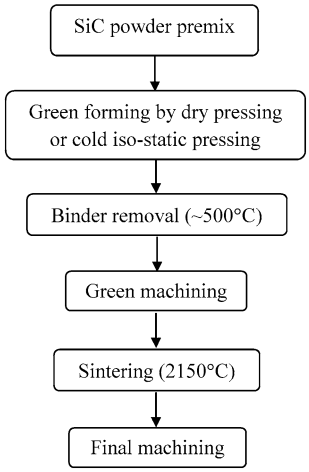

Fig. 1 Process flowchart diagram for producing S-SiC ceramics by powder metallurgy technique

Vargas-Gonzalez and Speyer (Ref 16) reported higher flexural strength and fracture toughness in S-SiC produced by hot-pressing technique compared to the SiC ceramics by pressureless sintering. Wereszczak et al. (Ref 17) investigated the effect of size-scaling and surface condition on the tensile strength of hot-pressed SiC. The authors observed a substantial decrease in characteristic strength (i.e., the strength of a body with unit volume at a failure probability of 0.632) with the increase in surface area for two different types of specimens prepared by surface grinding and surface grinding followed by grit blasting, respectively. The authors also predicted that the machining damage is the dominant flaw in the specimens with the effective area ranging between 0.1 and 40, 000 mm^2. Scafe et al. (Ref 13) reported the mechanical properties and fracture behavior of Si/SiC composites prepared by reaction sintering process. They showed that the size of the Si inclusion in the microstructure of composites was in agreement with the estimated size of critical flaw.

The present study aims at the investigation of the mechanical properties of S-SiC, failure statistics and the origin of flaws that leads to their failure. We report the preparation of S-SiC by dry pressing followed by pressureless sintering in the temperature range 1950-2180 °C in the presence of B_4C and C additives. The variation of density, phase(s), microstructure and mechanical properties with the increase in sintering temperature are discussed. The size of critical flaws in machined S-SiC parts with about 98% relative density (RD) is estimated with the help of measured mechanical properties and compared with the defects on the machined surfaces by SEM studies. Also, the failure behavior of S-SiC is investigated with the help of Weibull statistics.

2. Materials and Methods

2.1 Raw Materials and Powder Processing

The study was carried out using commercial grade α-SiC powder (Densitec 15, Saint-Gobain Ceramic Materials, Norway) as the starting material. The powder was spray dried premix granules which contains phenolic resin as the binder that not only provides strength to the green bodies but also yields carbon additive (3 wt.% approx.) while heat-treated in an inert atmosphere. This powder also contains about 1 wt.% of B_4C as another sintering additive and 0.75% SiO_2, 0.005% free Si as impurities in addition to 0.20% free C, 0.85% total oxygen and $<$ 700 ppm of trace elements including Fe, Al, Ni, V, Na, Cr, Ca, Ti, Mg and K. SiC green compacts were made by uniaxial pressing at 80 MPa using a steel die. Thereafter, the compacts were heat-treated in an atmosphere-controlled vacuum furnace at 500 °C for 1 h to effect the removal of organic volatiles and the conversion of phenolic resin to C. Subsequently, the specimens were sintered at different temperatures: 1950, 2050, 2150 and 2180 °C for 1 h in a vacuum sintering furnace in argon atmosphere. The heating rates used were 8 °C/min up to 1600 °C and subsequently 6 °C/min to the sintering temperature.

2.2 Material Characterizations

Bulk density (BD) measurement was taken by Archimedes principle (ASTM C372) with the help of an electronic balance (Make: Sartorius, Model: CP 225D, AG Gottingen, Germany) using deionized water as the immersion medium. Density data were averaged for more than five samples. The phase composition of raw SiC powder as well as the powder made from S-SiC was determined by utilizing an x-ray powder diffractometer (Bruker D8 Advance, Germany) equipped with copper $K_{\alpha 1}$ radiation (0.15418 nm wavelength) source and nickel monochromator. Microstructural analysis of polished and thermally etched as well as fracture surfaces was performed using a scanning electron microscope (S-3400 N, Hitachi, Japan) with secondary electron mode.

2.3 Mechanical Characterization

Four-point bending test was conducted for determination of flexural strength in a universal testing machine (UTM, Instron 4483, UK) over a span length and crosshead speed of 40 mm and 0.5 mm min^{-1}, respectively. The specimens (49 mm × 7.5 mm × 4 mm) were prepared by sectioning of SiC tiles (50 mm × 50 mm × 8 mm) followed by surface grinding to achieve the dimensional accuracy and removal of the sharp edges and corners of the specimens. The surface grinding was carried out using a 175-mm-diameter diamond gritted wheel (150 grit size) at about 10,000 rotations per minute (RPM) speed by maintaining a depth of cut of less than 8 μm in each cycle of the operation. Reported flexural strength data were averaged over minimum twelve specimens.

The Vickers hardness (HV) was measured using a microhardness tester (UHL VMHT, GmbH) equipped with a diamond indenter with a dwell time of 20 s. Vickers hardness was determined from the imprint size of the indenter as per the following equation (Ref 18):

$$\mathrm{HV} = 1.854\frac{P}{d^2} \qquad \text{(Eq 1)}$$

where P is the applied load and d is the mean length of two diagonal lines of the indentation imprint. The HV values reported here are the average of at least fifteen indentations. Fracture toughness (K_{IC}) was measured employing single-edge notch beam (SENB) technique. The specimens were of the same size to that of the four-point flexural tests but with a notch of about one-third thickness at the middle. Three-point bending test was conducted on the notched specimen

using a universal testing machine, and the strength data were used for the purpose of estimating the K_{IC} as per the following equation (Ref 18):

$$K_{IC} = \sigma_f Y \sqrt{c} \quad \text{(Eq 2)}$$

where c is the depth of notch, σ_f is the three-point flexural strength, and Y is the geometric parameter. The mathematical expression of Y for single-edge notch beam (SENB) method by three-point bending is expressed as follows (Ref 18):

$$Y = 1.93 - 3.07\left(\frac{c}{h}\right) + 14.53\left(\frac{c}{h}\right)^2 - 25.11\left(\frac{c}{h}\right)^3 + 25.8\left(\frac{c}{h}\right)^4 \quad \text{(Eq 3)}$$

where is h is the thickness of the specimen. The Young's modulus of the sintered specimen was measured by impulse excitation technique (IET) using Buzz-O-Sonic (model 5.8, Glendale, WI, USA) elastic modulus measurement instrument. Measurements were taken on 100-mm-diameter circular disk having 14 mm thickness. Weibull modulus was estimated with the help of Weibull statistics through analysis of four-point flexural strength data over a minimum of forty un-notched specimens.

3. Results and Discussion

3.1 Density, Phase and Microstructure

The BD of S-SiC densified at different temperatures is shown in Table 1. It can be observed that the BD increases from 2.17 g cm^{-3} (67.7% RD) at 1950 °C to the maximum of 3.16 g cm^{-3} (98.4% RD) at 2150 °C. It is also observed that the S-SiC heat-treated at 2180 °C showed the same BD to that of the specimens sintered at 2150 °C. Therefore, it could be predicted that the increase in sintering temperature beyond 2150 °C does not induce further densification in SiC in the presence of B and B_4C additives through pressureless sintering. The comparison between the x-ray diffraction (XRD) patterns of the starting powder and S-SiC specimen sintered 2150 °C is shown in Fig. 2. It is observed that the XRD patterns of both the materials correspond to polycrystalline α-SiC (hexagonal). It is also observed that the α-phase in S-SiC consists of 6H and 4H polytypes compared to that of only 6H polytype in the starting powder. This could be attributed to the existence of a large number of polytypic modifications (Ref 19, 20) of SiC based on the hexagonal unit cell with the same basal plane but only differing in the stacking of unit layers along the c-axis. The low free energy differences among the various SiC polytypes affected the transformation of 6H polytypes to 4H during densification. The phase composition in S-SiC sintered at 1950, 2050 and 2180 °C (XRD patterns not shown in Fig. 2 for simplicity) is also observed to be the same to that of the specimens sintered at 2150 °C.

The SEM micrographs at lower magnification on the polished surfaces of S-SiC densified at different temperatures are shown in Fig. 3. The distribution of residual pores is found to be uniform in all the samples. It is also observed from the micrographs (Fig. 3) that the specimens sintered at higher temperature exhibited smoother surfaces which is in agreement with the BD. The changes in microstructure with the increase in sintering temperature are shown in Fig. 4. The increase in sintering temperature gradually decreased the overall porosity and increased the intergranular bonding which are also in agreement with the BD results. It can be observed from Fig. 4(a) that S-SiC sintered at 1950 °C consists of loosely bonded small size grains as the specimen exhibited only 67.7% RD. The increase in RD to 91.0% through the increase in sintering temperature to 2050 °C resulted in the microstructure with decreased porosity and well developed faceted gains (Fig. 4b). The increase in sintering temperature to 2150 °C increased the RD to 98.4%, and the microstructure (Fig. 4c) shows further decrease in porosity and noticeably higher size interconnected duplex grains (equiaxed and elongated). The microstructure of S-SiC sintered at 2180 °C (Fig. 4d) is found to be comparable to that of the 2150 °C microstructure but with slightly higher grains.

The densification behavior of SiC in the absence of any secondary phase was first demonstrated by Prochazka (Ref 10) using B and C additives. However, the role of B and C in influencing mass transport mechanism for the densification of SiC has not been understood completely, although SiC densification due to the reduction of grain boundary energy

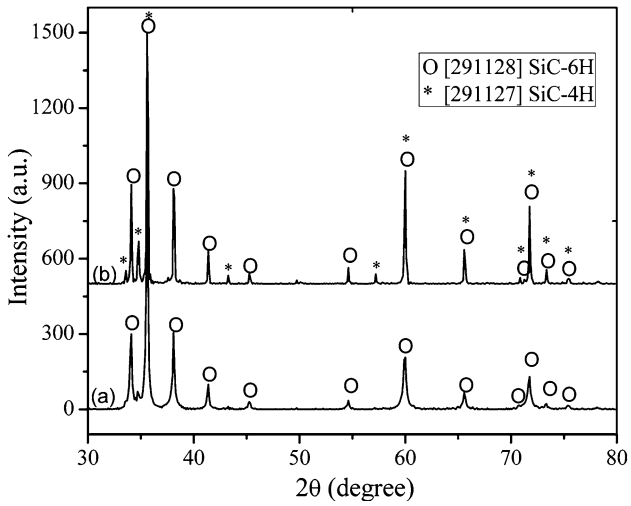

Fig. 2 X-ray diffraction (XRD) pattern of (a) raw SiC powder and (b) S-SiC sintered at 2150 °C

Table 1 Bulk density (BD) of S-SiC sintered at different temperatures

Sintering temperature	1950 °C	2050 °C	2150 °C	2180 °C
Bulk density (BD, g cm^{-3})*	2.17	2.92	3.16	3.16
Relative density (RD%)	67.6	91.0	98.4	98.4

*Uniaxially compacted green specimens exhibited the density of 1.75 g cm^{-3} (54.5% RD)

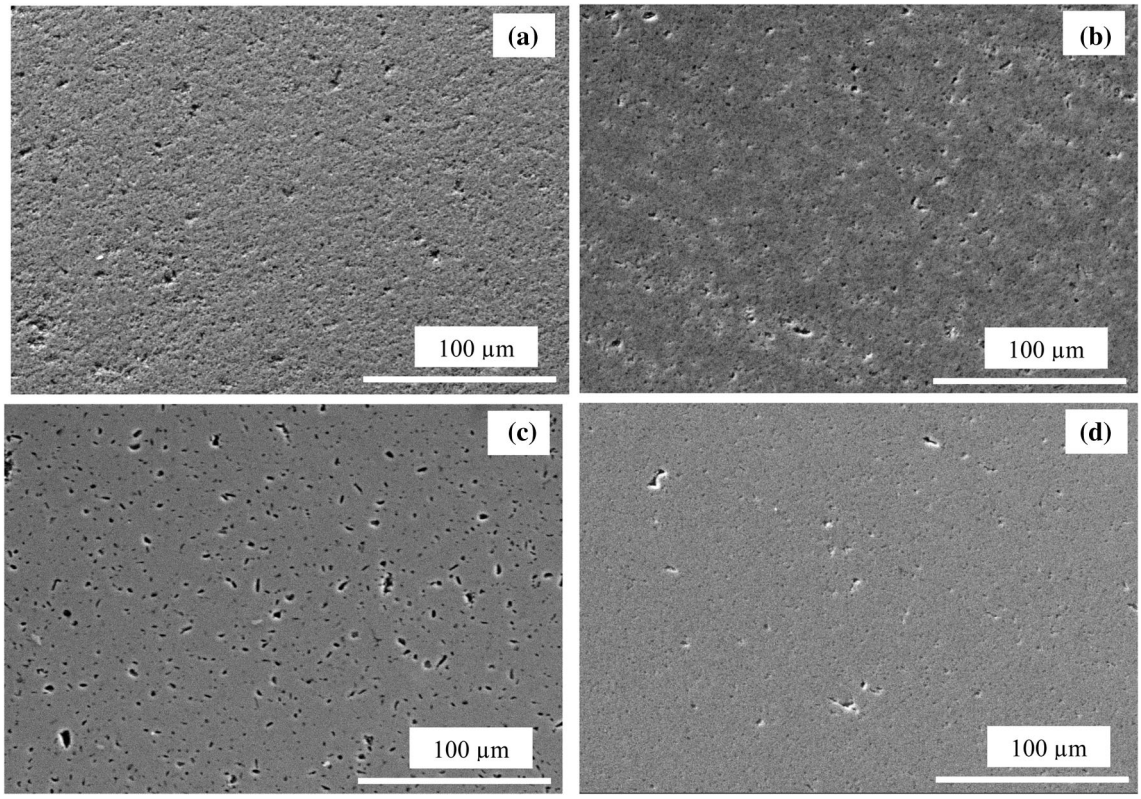

Fig. 3 SEM micrograph of on the polished surfaces of S-SiC sintered at (a) 1950 °C, (b) 2050 °C, (c) 2150 °C and (d) 2180 °C

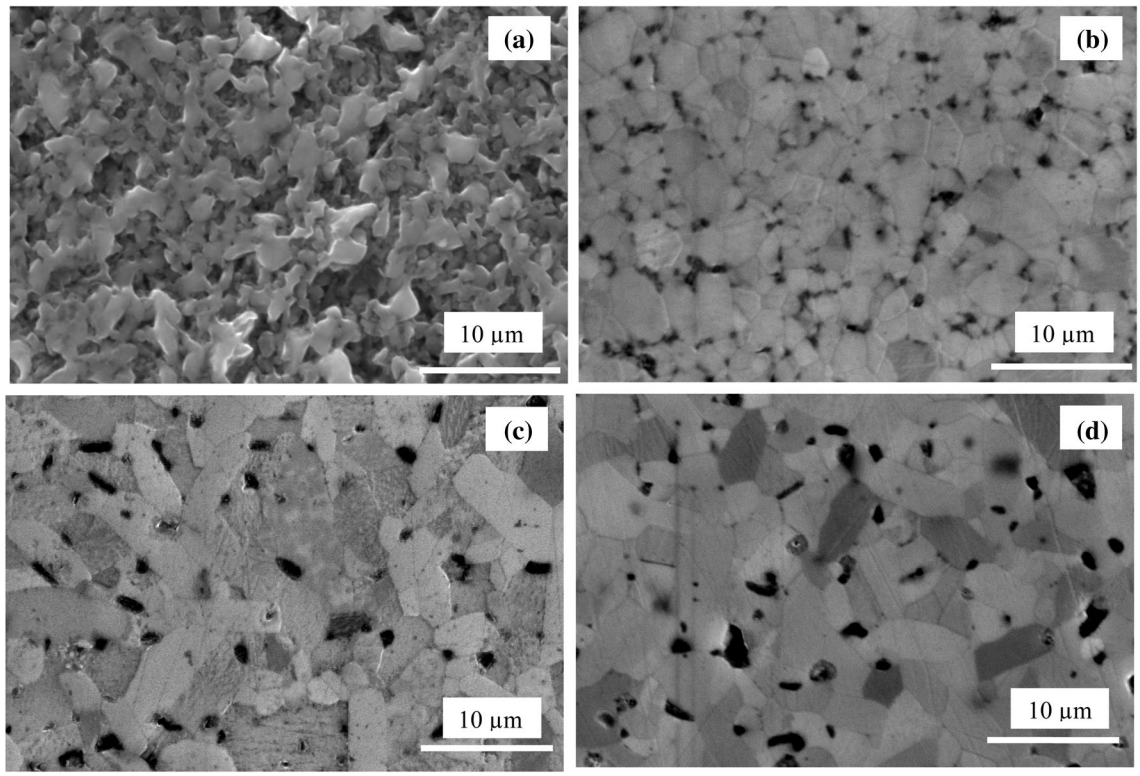

Fig. 4 SEM micrograph of on thermally etched surfaces of S-SiC sintered at (a) 1950 °C, (b) 2050 °C, (c) 2150 °C and (d) 2180 °C

(Ref 10, 21), the transient liquid phase sintering (Ref 22, 23) and the activation of grain boundary diffusion (Ref 24) are reported in the literature. Irrespective of the exact densification mechanism (s) prevailed, the present study demonstrates that the SiC ceramics can be densified to 98.4% RD through pressureless sintering at 2150 °C.

3.2 Mechanical Properties

The mechanical properties, i.e., flexural strength (four-point) and Vickers hardness of S-SiC sintered at different temperatures, are shown in Table 2. It can be observed from the Table 2 that the increase in sintering temperature in the range of 1950-2150 °C increased both the mechanical properties. The maximum strength and hardness of 219 ± 22 MPa and 2530 ± 80 kg mm^{-2}, respectively, are observed in the S-SiC parts sintered at 2150 °C. The increase in RD with the increase in the sintering temperature (1950-2150 °C) reduced the porosity and increased intergranular bonding which in turn resulted in the higher mechanical properties. In spite of the same RD, the reason for slightly lower mechanical properties in the S-SiC sintered at 2180 °C than 2150 °C (Table 2) could be attributed to the grain size (Fig. 4d and c, respectively). Following the results presented in this section, it can be understood that the S-SiC parts sintered at 2150 °C show the better combination of density, microstructure and mechanical properties compared to that of at other temperatures. Subsequently, detailed studies on the indentation and fracture behavior and the origin of strength-limiting flaws in the S-SiC parts sintered at 2150 °C are discussed below.

Figure 5 shows the effect of indentation load on HV of S-SiC specimens sintered at 2150 °C. As seen from Fig. 5, HV of S-SiC decreases with the increase in indentation load and it exhibited HV of 2530 kg mm^{-2} at 500 g load. The decrease in HV with the increase in load (known as indentation size effect, ISE) is explained based on the elastic–plastic model of discrete deformation bands in high hardness materials including SiC (Ref 25, 26). According to this model, the size of an indentation imprint is the combined effect of elastic recovery and plastic deformation. This model also assumes that the extent of elastic recovery is relatively higher at low indentation load compared to the formation of a new plastic zone. Therefore, a relatively smaller indentation imprint at low load resulted in higher HV.

Fracture toughness (K_{IC}) of S-SiC sintered at 2150 °C by SENB technique is found to be 3.43 MPa m$^{1/2}$. Although SiC exhibits relatively higher toughness compared to other ceramics (Ref 9, 16), it is also brittle and fails catastrophically. Brittle fracture in S-SiC (densified at 2150 °C) is evidenced in the fracture surface SEM micrograph in Fig. 6. As can be seen from Fig. 6, S-SiC exhibited transgranular fracture without showing any plastic deformation. The inherent brittle behavior of SiC is associated with the presence of strong directional covalent bonds which inhibits plastic deformation even in the presence of high mechanical stress (Ref 15). For the sake of completeness in mechanical properties of S-SiC sintered at 2150 °C, the measured value of Young's modulus by IET method is found to be 422 GPa which is in agreement with the literature (Ref 2).

Table 2 Vickers hardness and flexural strength of S-SiC sintered at different temperatures

Sintering temperature	Flexural strength, MPa	Vickers hardness, HV, kg mm^{-2}
1950 °C	92 ± 12	642 ± 72
2050 °C	175 ± 25	20.46 ± 80
2150 °C	219 ± 22	2530 ± 80
2180 °C	213 ± 26	2488 ± 98

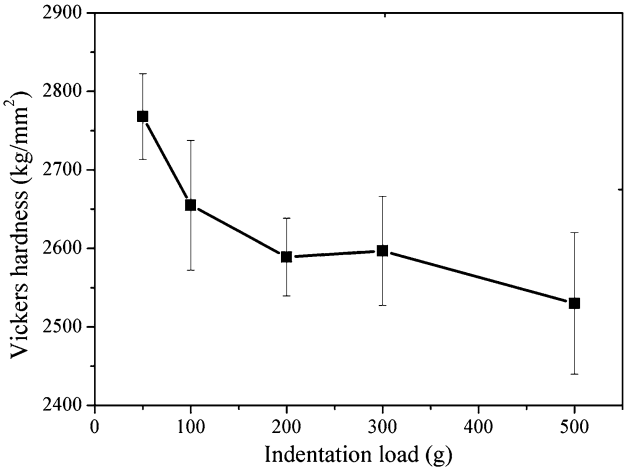

Fig. 5 Relation of Vickers hardness (HV) of S-SiC with indentation load

3.3 Surface Defects and Critical Flaw Size

The failure of SiC-based ceramics is normally associated with the presence of preexisting flaws including cracks, voids and microstructural defects that cause the stress concentration by subjecting the body under the influence of mechanical load. The general relationship between stress intensity factor (K) and applied stress (σ) can be expressed as per the following equation (Ref 18):

$$K = \sigma Y \sqrt{c} \quad \text{(Eq 4)}$$

where c is the flaw size and Y is a dimensionless parameter which depends on the type of loading and the crack geometry. It is evident from Eq 4 that the largest flaw in a body causes the highest stress concentration and eventually limits the strength which is analogous to the weakest link of a chain. As the severity of surface cracks is greater than any other defects, we estimated the critical flaw size by considering non-interacting semi-elliptical surface crack as per the following equation (Ref 18):

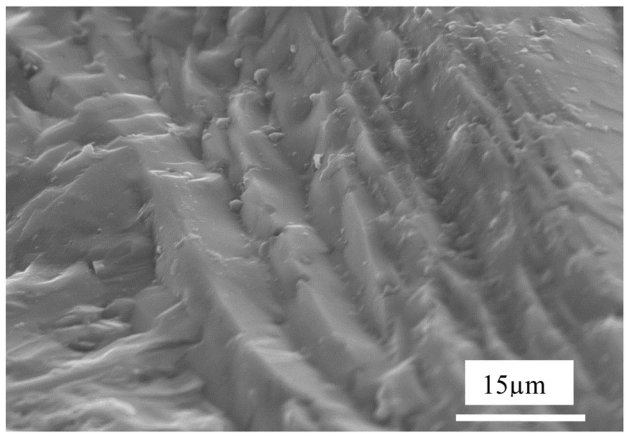

Fig. 6 SEM micrograph of the fracture surface of S-SiC densified at 2150 °C

$$c = \frac{1}{1.25\pi}\left(\frac{K_{IC}}{\sigma_f}\right)^2 \quad \text{(Eq 5)}$$

where σ_f is the fracture strength. Equation 5 is a special form of Eq 4 at the point of failure where the value of Y is 1.12 for a semi-elliptical surface crack. Based on the measured four-point flexural strength (σ_f in the range of 177-272 MPa) and K_{IC} (3.43 MPa $m^{1/2}$) of S-SiC densified at 2150 °C, the estimated critical crack size in our study varied between 32 and 110 μm.

The genesis of flaws and their population in brittle materials like SiC is attributed to the processed microstructure, e.g., impurities, hard agglomerates, pores, voids. Also, the most severe surface cracks are introduced during machining operations including sectioning and surface grinding or even during handling. The estimated critical flaw sizes in our study are much greater than any of the microstructural feature. Therefore, it can be predicted that the critical flaws might have originated from machining operations associated with the specimen preparation (Ref 27, 28). The SEM micrograph on machined surfaces of S-SiC (sintered at 2150 °C) in Fig. 7(a) reveals the distribution of surface defects including particle pullouts and surface cracks. It can also be observed from Fig. 7(a) that the order of magnitude of such defects is comparable to the crack size estimated from Eq 5. Although the length of some surfaces cracks (e.g., ~ 38 μm in Fig. 7b) falls well within the range of estimated flaws, the size of critical flaws as per Eq 5 is considered to represent the depth of the non-interacting semi-elliptical surface crack. However, the accuracy in determining critical flaw size depends on the exact geometry of surface cracks, the mode of fracture (orientation of the crack surface with loading direction) and defects interaction.

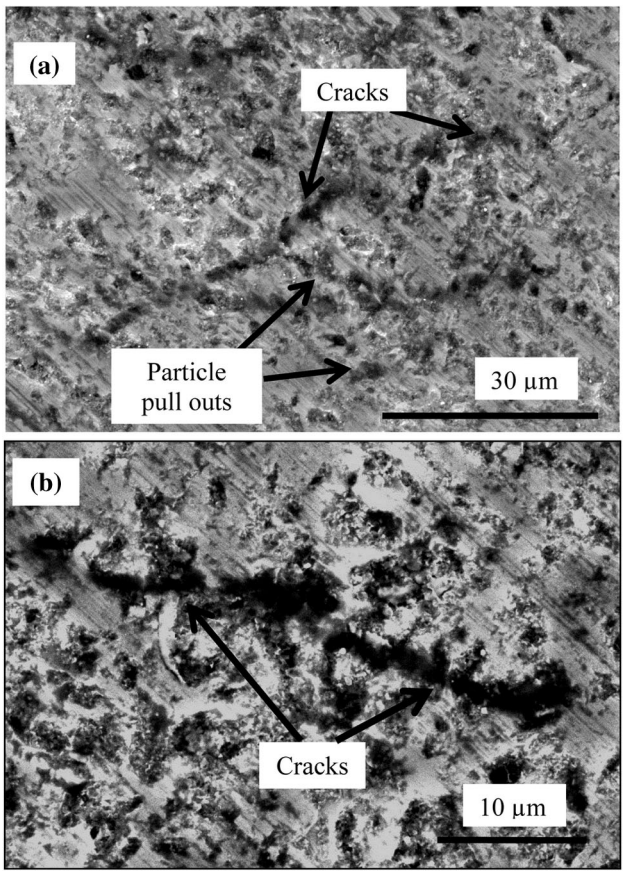

Fig. 7 SEM micrograph of machined surfaces of 2150 °C sintered S-SiC: (a) surface defects including distribution of cracks and (b) with a surface crack of length ~ 38 μm

3.4 Weibull Statistics

The variation of strength in brittle materials could be analyzed with the help of various statistical approaches including generalized exponential relationship, log-normal, Weibull and gamma distribution to predict the probability of failure (Ref 29). We applied commonly used two-parameter Weibull distribution to analyze the probability of failure using four-point flexural strength data of S-SiC sintered at 2150 °C. Following is the expression for two-parameter Weibull distribution (Ref 18):

$$\ln\ln\left(\frac{1}{1-F}\right) = m\ln\sigma_f - m\ln\sigma_0^* \quad \text{(Eq 6)}$$

where F is the probability of failure, σ_f is the fracture strength, σ_0^* is the scaling parameter, and m is the Weibull modulus. The probability of failure F is estimated as per the following equation:

$$F = \frac{j}{N+1} \quad \text{(Eq 7)}$$

where j is the j^{th} specimen in a group of N specimens ranked in the order of increasing fracture strength. The plot of a double logarithmic left-hand side of Eq 6 versus $\ln\sigma_f$, Weibull plot, is shown in Fig. 8, and m is determined from the slope of the best fit straight line. A high m value is an indicator of the uniform distribution of critical flaws with the high degree of reliability of parts in service and vice versa. Based on the varied strength between 177 and 272 MPa (with the average of 219 MPa and the standard deviation of 22 MPa), we obtained the Weibull modulus 11.2 in the S-SiC ceramics sintered at 2150 °C, in agreement with the literature (Ref 17, 30).

The effect of processing conditions and specimen size on the Weibull modulus are well reported in the literature. Dongliang

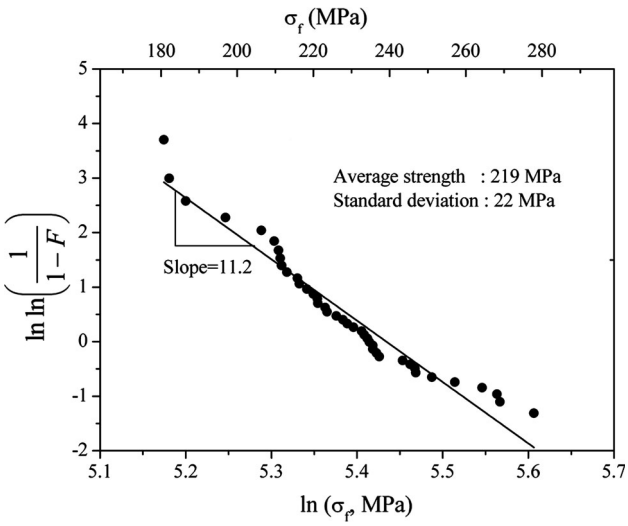

Fig. 8 Weibull plot of four-point bending strength of S-SiC sintered at 2150 °C

and Jihong (Ref 30) reported that post-hipping of 92% RD S-SiC for 1 h increased the density to 98% RD and fracture strength by 18% without any positive effect on the Weibull modulus. Although the post-hipping treatment resulted in reduced porosity and pore size, the distribution of strength-limiting defects, e.g., agglomerates, inclusions, second phases, etc., remained unchanged. The authors also reported the increase in the Weibull modulus by longtime annealing of hot isostatically pressed (HIPed) S-SiC specimens. The increase in the Weibull modulus in hot-pressed S-SiC by control of microstructure through crack-bridging is also reported (Ref 16). Wereszczak et al. (Ref 17) reported that the Weibull modulus for hot-pressed SiC decreased with the decrease in the effective area of the specimens due to the multiple distributions of flaws in a given range of specimen size (in terms of area). Irrespective of anomalous results in certain cases, a given value of the Weibull modulus corresponds to a particular distribution of flaws depending on the materials behavior and its processing history. The Weibull modulus observed in our study is attributed to the distribution of surface defects originated from machining. Therefore, the failure behavior of S-SiC parts produced by pressureless sintering followed by machining could be predicted from the distribution of surface defects.

4. Conclusions

Densified S-SiC ceramics with the maximum of 98.4% RD were prepared in the presence of B_4C and C as additives through pressureless sintering at 2150 °C and above. The increase in sintering temperature in the range of 1950-2150 °C increased the density of S-SiC through the removal of porosity and increase in intergranular bonding which resulted in the increase in mechanical properties including flexural strength and hardness. X-ray diffraction study shows that the sintered SiC consisted of polycrystalline α-phase in the form of 4H and 6H polytypes. Fracture surface scanning electron micrograph of S-SiC densified at 2150 °C reveals the brittle fracture. Based on the flexural strength and fracture toughness of 2150 °C sintered S-SiC, the size of the critical flaw on the machined surfaces ranges between 32 and 110 μm. The size of critical flaws is found to be comparable with the order of magnitude of surface defects. The failure behavior of macroscopic S-SiC parts is predicted from the distribution of strength-limiting surface flaws generated through machining operations.

References

1. K. Yamada and M. Mohri, Properties and Applications of Silicon Carbide Ceramics, *Silicon Carbide Ceramics-1: Fundamentals and Solid Reaction*, S. Somiya and Y. Inomata, Ed., Elsevier Applied Science, New York, 1991, p 13–44
2. H. Tanaka, Silicon Carbide Powder and Sintered Materials, *J. Ceram. Soc. Jap.*, 2011, **119**, p 218–233
3. S. Goel, The Current Understanding of the Diamond Machining of Silicon Carbide, *J. Phys. D Appl. Phys.*, 2014, **47**, p 1–36
4. M. Omori and H. Takei, Preparation of Pressureless Sintered SiC-Al_2O_3-Y_2O_3, *J. Mater. Sci.*, 1998, **23**, p 3744–3749
5. E.V. Zaretsky, Ceramic Bearings for Use in Gas Turbine Engines, *J. Mater. Eng. Perform.*, 2013, **22**, p 2830–2846
6. M.A. Mulla and V.D. Krstic, Mechanical Properties of β-SiC Pressureless Sintered with $A1_2O_3$ Additions, *Acta Metall. Mater.*, 1994, **42**, p 303–308
7. J.J. Melendez-Martinez, M. Castillo-Rodriguez, and A. Dominguez-Rodriguez, Creep and Microstructural Evolution at High Temperature of Liquid Phase-Sintered Silicon Carbide, *J. Am. Ceram. Soc.*, 2007, **90**, p 163–169
8. J. Chen, N. Li, Y. Wei, H. Han, and W. Yan, Effect of Ferrosilicon Additive and Sintering Condition on Microstructural Evolution and Mechanical Properties of Reaction-Bonded SiC Refractories, *Ceram. Inter.*, 2016, **42**, p 17650–17658
9. D.D. Nesmelov and S.N. Perevislov, Reaction Sintered Materials Based on Boron Carbide and Silicon Carbide, *Glass Ceram.*, 2015, **71**, p 313–319
10. S. Prochazka, The Role of Boron and Carbon in the Sintering of Silicon Carbide, *Special Ceramics*, 6th ed., P. Popper, Ed., British Ceramic Research Association, Stoke-on Trent, 1975, p 171–182
11. A. Gubernat, L. Stobierski, and P. Łabaj, Microstructure and Mechanical Properties of Silicon Carbide Pressureless Sintered with Oxide Additives, *J. Eur. Ceram. Soc.*, 2007, **27**, p 781–789
12. Y. Hirata, N. Matsunaga, and S. Sameshima, Densification, Phases, Microstructures and Mechanical Properties of Liquid Phase-Sintered SiC, *Key Eng. Mater.*, 2011, **484**, p 124–129
13. E. Scafe, G. Giunta, L. Fabbri, L.D. Rese, G.D. Portu, and S. Guicciardi, Mechanical Behaviour of Silicon-Silicon Carbide Composites, *J. Eur. Ceram. Soc.*, 2011, **16**, p 703–713
14. G. Zhan and M. Mitomo, Microstructural Control for Strengthening of Silicon Carbide Ceramics, *J. Am. Ceram. Soc.*, 1992, **82**, p 2924–2926
15. S. Kaur, R.A. Cutler, and D.K. Shetty, Short-Crack Fracture Toughness of Silicon Carbide, *J. Am. Ceram. Soc.*, 2009, **92**, p 179–185
16. L. Vargas-Gonzalez and R.F. Speyer, Flexural Strength, Fracture Toughness and Hardness of Silicon Carbide and Boron Carbide armour Ceramics, *Inter. J. Appl. Ceram. Technol.*, 2010, **7**, p 643–651
17. A.A. Wereszczak, T.P. Kirkland, and K.T. Strong, Jr., Size-Scaling of Tensile Failure Stress in a Hot-Pressed Silicon Carbide, *Inter. J. Appl. Ceram. Technol.*, 2010, **7**, p 635–642
18. D.J. Green, *An Introduction to Mechanical Properties of Ceramics*, 1st ed., Cambridge University Press, New York, 1998, p 189–292
19. L.A. Ortiz, F. Sanchez-Bajo, F.L. Cumbrera, and F. Guiberteau, X-ray Powder Diffraction Analysis of a Silicon Carbide Based Ceramics, *Mater. Lett.*, 2001, **49**, p 137–145
20. D. Pandey and P. Krishna, The Origin of Polytype Structures, *Prog. Cryst. Growth Ch. Mater.*, 1983, **7**, p 213–258
21. W.J. Clegg, Role of Carbon in the Sintering of Boron-Doped Silicon Carbide, *J. Am. Ceram. Soc.*, 2000, **83**, p 1039–1043
22. A. Gubernat and L. Stobierski, Sintering of Silicon Carbide I. Effect of Carbon, *Ceram. Inter.*, 2003, **29**, p 287–292
23. F.F. Lange and T.K. Gupta, Sintering of SiC with Boron Compounds, *J. Am. Ceram. Soc.*, 1976, **59**, p 537–538
24. A. Malinge, A. Coupe, Y. Petitcorps, and R. Pailler, Pressureless Sintering of Beta-Silicon Carbide Nanoparticles, *J. Euro. Ceram. Soc.*, 2012, **32**, p 4393–4400
25. S.J. Bull, T.F. Page, and E.H. Yoffe, An Explanation of the Indentation Size Effect in Ceramics, *Phil. Mag. Lett.*, 1989, **59**, p 281–288
26. P. Barick, D.C. Jana, and B.P. Saha, Load-Dependent Indentation Behaviour of β-SiAlON and α-Silicon Carbide, *J. Adv. Ceram.*, 2013, **2**, p 185–192
27. B. Zhang, X.L. Zheng, H. Tokura, and M. Yoshikawa, Grinding Induced Damage in Ceramics, *J. Mater. Process. Technol.*, 2003, **132**, p 353–364
28. J. Cao, Y. Wu, D. Lu, M. Fujimoto, and M. Nomura, Fundamental Machining Characteristics of Ultrasonic Assisted Internal Grinding of SiC Ceramics, *Mater. Manuf. Process.*, 2014, **29**, p 557–563
29. B. Basu, D. Tiwari, D. Kundu, and R. Prasad, Is Weibull Distribution the Most Appropriate Statistical Strength Distribution for Brittle Materials?, *Ceram. Inter.*, 2009, **35**, p 237–246
30. S. Jihong and J. Dongliang, Hot Iso-static Pressing of Presintered Silicon Carbide Ceramics, *J. Eur. Ceram. Soc.*, 1991, **7**, p 243–247